



Hyperchaos and synchronization in two element nonlinear chimney model

Cite as: Chaos 30, 123114 (2020); <https://doi.org/10.1063/5.0015488>

Submitted: 28 May 2020 . Accepted: 05 November 2020 . Published Online: 02 December 2020

 Anisha R. V. Kashyap, and  Kiran M. Kolwankar



View Online



Export Citation



CrossMark

**Certified as
TRUE COPY**

Principal
Ramniranjan Jhunjhunwala College,
Ghatkopar (W), Mumbai-400086.

NEW!

Sign up for topic alerts
New articles delivered to your inbox



PRINCIPAL
RAMNIRANJAN JHUNJHUNWALA COLLEGE
OF ARTS, SCIENCE & COMMERCE (AUTONOMOUS)
Ghatkopar (W), Mumbai-400 086, Maharashtra, INDIA

Hyperchaos and synchronization in two element nonlinear chimney model

Cite as: Chaos 30, 123114 (2020); doi: 10.1063/5.0015488

Submitted: 28 May 2020 · Accepted: 5 November 2020 ·

Published Online: 2 December 2020



View Online



Export Citations



CrossMark

Anisha R. V. Kashyap^{1,2,a)} and Kiran M. Kolwankar²

AFFILIATIONS

¹Department of Physics, University of Mumbai, Santa Cruz (E), Mumbai 400 098, India

²Department of Physics, Ramniranjan Jhunjhunwala College, Ghatkopar (W), Mumbai 400 086, India

^{a)}Authors to whom correspondence should be addressed: anisha.kashyap27@gmail.com and Kiran.Kolwankar@gmail.com

ABSTRACT

The two element chimney model with nonlinearity is studied with the aim of modeling the swaying of trees at high wind speeds. We found solutions for various parameters and also the Lyapunov spectrum numerically. The system is chaotic for a wide range of parameters. We also observed hyperchaos in a subregion of this parameter space. We noticed that the hyperchaos was suppressed when the largest Lyapunov exponent crossed a threshold value. Synchronization between the lower and the upper segments was also studied and, for some parameters, phase synchronization is observed. We also observed transition to antisynchronization and also toggling between the two as the parameters are varied.

Published under license by AIP Publishing. <https://doi.org/10.1063/5.0015488>

The swaying motion of trees has been the subject of several investigations, theoretical as well as experimental, by forest scientists. The reasons for their interest are obviously driven by the losses incurred in stormy conditions. Another place where the understanding of the equations governing the motion of trees is needed is computer animation. The reduced set of equations describing a moving tree will definitely speed up this task, especially when a large number of trees are involved. Though it is evident that the swaying motion of trees is a nonlinear phenomenon, surprisingly, not much effort has been invested in its complete nonlinear analysis. This work is part of such a program to build and understand a complete model step by step.

I. INTRODUCTION

Oscillation of trees driven by wind is always a matter of interest for a broad range of groups, such as forest scientists,¹⁻³ engineers,⁴ animators,⁵⁻⁷ etc. Their motivations are different, including minimizing damage in stormy wind conditions, improving the stability of the structures, or providing better and more realistic visuals. Trees have a very complex architecture that differs from tree to tree and shows very irregular behavior under high wind and can thus be cited as a natural example of the nonlinear system; but, the nonlinear behavior of this complex system has not been studied much in detail.

The experimental study on the motion of trees has been an active field of research. Several workers have measured various aspects of the movement of trees.⁸ They have used various techniques for this purpose, such as using a laser for tracking,⁹ measuring the inclination,¹⁰ or using motion tracking from videos,¹¹ etc.

Theoretically, the earlier attempts for understanding the swaying motion of trees mainly followed two approaches. First, the tree was approximated as a cantilever beam with corresponding partial differential equations describing free vibrations of its central column.¹²⁻¹⁴ Second, it was depicted as a chimney model consisting of coupled short oscillating sections with restoring forces at the joints.¹⁵ Both these models have been developed with the assumption that trees are a linear system and neither considered nonlinear restoring forces or even the branched structure.

Since it is known that biological materials exhibit a nonlinear response,¹⁶ the absence of nonlinearity in the models has been particularly striking. Relatively recently, some studies have been initiated that introduce nonlinearity in the restoring force.¹⁷ They considered a basic model consisting of one nonlinear oscillator, and its effect on the resonance was discussed. While some other study¹⁸ introduced a branched structure with nonlinearity in the model, it has not been analyzed much. In order to understand how branching helps in dissipating perturbation and increasing structural stability, Thecke *et al.*¹⁹ studied a Y-shaped branch structure, and Fankem *et al.*²⁰ carried out a work to test the pagoda system stability, but

Certified as
TRUE COPY

Principal

Ramniranjan Jhunjhunwala College,
Ghatkopar (W), Mumbai-400086.

both did not include nonlinearity. Thus, to summarize, studies were carried out with a simple nonlinear structure or with a complex structure but without nonlinearity. Very recently,²¹ an interesting study was carried out to explore the localization of vibrations in which a branched structure along with the nonlinear restoring forces was considered. However, this work did not include the gravitational force and also did not study the nonlinear dynamical properties of the system. In summary, while these studies have begun the introduction of nonlinear effects in the modeling of the swaying of trees, a systematic study with emphasis on nonlinear phenomena is still lacking. In fact, in Ref. 22, to generate better animation of irregular motion of trees, a driving with $1/f^\beta$ noise was introduced. In our work, we plan to explore an alternative source of irregularity that comes from the nonlinearity of the system.

In our previous work,²² we started the development of the nonlinear chimney model in order to study the swaying of trees. We made a systematic nonlinear analysis of this model and intend to compare the findings, if possible, with the experimental data. We have already discussed the nonlinear properties of this model's basic building block,²¹ that is, the single element chimney model. We also discussed approximate solutions to the equations of this model.²⁴ The present study is the next step in this endeavor. In this work, the focus is not on application to an actual tree but only on the nonlinear dynamical properties of the model that might be of relevance.

The paper is organized as follows. In Sec. II, we define the model. Then, in Sec. III, we explain our choice of the range of parameters explored in this work. This is followed by Sec. IV of numerical results explaining the chaotic properties present in this system like chaos, hyperchaos, and suppression of hyperchaos. In Sec. V, the synchronization between lower and upper segments is discussed. Finally, we end the paper with some concluding discussions.

II. THE MODEL

We consider the chimney model that was introduced previously¹⁵ but with linear restoring forces. We chose this model because later it would allow us to study branched structures easily. In this model, a tree is imagined to consist of N short segments connected end to end and perpendicular to the ground or another stiffer branch. Unlike in Ref. 15, we have considered nonlinear restoring forces acting between the segment joints and between the first segment and the base. There is also a gravitational force at the center of each segment, which is also nonlinear. The equation of motion for the N segments is derived using the Lagrangian formulation. In Ref. 23, we focused on this model's basic building block, i.e., the single element model. We found that this simple case showed chaotic behavior for some values of parameters. We also considered the two elements case briefly.

In this paper, we plan to study the case consisting of two elements in more detail. We will analyze this system for a wider

range of parameters and study the chaotic properties as well as the synchronization between two segments. It can be thought of as a generalization of a double pendulum with an addition of the restoring forces at the joints. Also, because the restoring forces in our model act in the opposite direction to that of the gravitational force, the equilibrium position here is different from that of the double pendulum. We have already derived the equation of motion for this system in Ref. 23. Here, we recall some important steps for the sake of completeness.

The Lagrangian for two segment system is

$$L_2 = \frac{1}{2} \dot{\theta}_1^2 \left(\frac{m_1}{4} + m_2 \right) + \frac{1}{2} \dot{\theta}_2^2 \left(\frac{m_2}{4} \right) + \ell^2 \dot{\theta}_1 \dot{\theta}_2 \cos(\theta_2 - \theta_1) \left(\frac{m_2}{2} \right) - g \ell \left(\frac{m_1}{2} + m_2 \right) \cos \theta_1 - g \ell \left(\frac{m_2}{2} \right) \cos \theta_2 - \frac{1}{2} k_1 \theta_1^2 - \frac{1}{4} k_1 \alpha_1 \theta_1^4 - \frac{1}{2} k_2 (\theta_2 - \theta_1)^2 - \frac{1}{4} k_2 \alpha_2 (\theta_2 - \theta_1)^4, \tag{1}$$

where θ_i is the angle of the i th segment with the vertical and m_i is the mass concentrated at the center. Here, we presume that both segments have the same length that is equal to ℓ . Also, k_i is the linear restoring coefficients and α_i is the nonlinear restoring coefficients for the i th element. Rayleigh's dissipation function for this system, assuming the dissipation along each direction is the same,

$$\mathcal{F}_2 = \frac{1}{2} b \ell^2 \left(\frac{5 \dot{\theta}_1^2}{4} + \frac{\dot{\theta}_2^2}{4} + \dot{\theta}_1 \dot{\theta}_2 \cos(\theta_2 - \theta_1) \right). \tag{2}$$

Now, let Q_1^{drive} and Q_2^{drive} be the driving forces in θ_1 and θ_2 directions, respectively. This driving force is due to the wind, which can have two different forms. When the direction of the wind is continuously changing, which resembles the situation of stormy wind, the Q_i^{drive} can be expressed by $\ell_i f \cos \omega t / 2$, and when the wind is flowing from a certain fixed direction, then this drive can be represented by $\ell_i (d + f \cos \omega t) \cos \theta_i / 2$, where d is the average force in a given direction; we have multiplied by $\cos \theta_i$ as we need the component in the horizontal direction. We have studied the single element system in Ref. 23 by considering both types of wind but here, for the two element system, we restrict ourselves to the former case of wind. Thus, $Q_1^{drive} = \ell_1 f \cos \omega t / 2$ and $Q_2^{drive} = \ell_2 f \cos \omega t / 2$. Since $\ell_1 = \ell_2 = \ell$, these drives on each segment will be the same, and hence, $Q_1^{drive} = Q_2^{drive} = \ell f \cos \omega t / 2$.

Now, if we write down the Lagrange equations for the two variables θ_1 and θ_2 , then after some algebra and substituting $\ell = 1$, $m_1 = m_2 = 1$, we arrive at

$$\ddot{\theta}_1 = \left(\frac{1}{1 - \frac{4}{5} \cos(\theta_2 - \theta_1)^2} \right) \left(\frac{4}{5} \dot{\theta}_1^2 \sin(\theta_2 - \theta_1) \cos(\theta_2 - \theta_1) - \frac{4}{5} g \sin \theta_2 \cos(\theta_2 - \theta_1) + \frac{8}{5} k_2 (\theta_2 - \theta_1) \cos(\theta_2 - \theta_1) (1 + \alpha_2 (\theta_2 - \theta_1)^2) + \frac{4}{5} b \dot{\theta}_1 \cos(\theta_2 - \theta_1)^2 - \frac{4}{5} f \cos \omega t \cos(\theta_2 - \theta_1) \right)$$

$$\begin{aligned}
 & + \frac{2}{5}\dot{\theta}_2^2 \sin(\theta_2 - \theta_1) + \frac{6}{5}g \sin \theta_1 - \frac{4}{5}k_1\theta_1(1 + \alpha_1\theta_1^2) + \frac{4}{5}k_2(\theta_2 - \theta_1)(1 + \alpha_2(\theta_2 - \theta_1)^2) \\
 & - b\dot{\theta}_1 + \frac{2}{5}f \cos \omega t, \tag{3}
 \end{aligned}$$

$$\begin{aligned}
 \ddot{\theta}_2 = & \left(\frac{1}{1 - \frac{4}{5}\cos(\theta_2 - \theta_1)^2} \right) \left(-\frac{4}{5}\dot{\theta}_2^2 \sin(\theta_2 - \theta_1) \cos(\theta_2 - \theta_1) - \frac{12}{5}g \sin \theta_1 \cos(\theta_2 - \theta_1) \right. \\
 & + \frac{8}{5}k_1\theta_1 \cos(\theta_2 - \theta_1)(1 + \alpha_1\theta_1^2) - \frac{8}{5}k_2(\theta_2 - \theta_1) \cos(\theta_2 - \theta_1)(1 + \alpha_2(\theta_2 - \theta_1)^2) \\
 & + \frac{4}{5}b\dot{\theta}_2 \cos(\theta_2 - \theta_1)^2 - \frac{4}{5}f \cos \omega t \cos(\theta_2 - \theta_1) - 2\dot{\theta}_1^2 \sin(\theta_2 - \theta_1) + 2g \sin \theta_2 \\
 & \left. - 4k_2(\theta_2 - \theta_1)(1 + \alpha_2(\theta_2 - \theta_1)^2) - b\dot{\theta}_2 + 2f \cos \omega t \right). \tag{4}
 \end{aligned}$$

These are the equations of motion for the two segment system. Generally, the width decreases as one goes up on a tree. This varying width can be modeled by different masses of the segments. Here, we have chosen the masses to be the same, which is a valid approximation for some plants, especially when it is divided just in two segments.

III. POTENTIAL ENERGY

Our system involves many parameters. The potential energy itself has four of them, k_1 , α_1 , k_2 , and α_2 . Studying the system with a variation in all of them in all possible ranges will be a Herculean task. Clearly, one needs to carefully identify different classes of the ranges of parameters and study the system separately in different classes. In fact, the different ranges of the parameters assign different stiffness properties to the trees and their different parts. As a result, these classes might in fact lead to a reasonable classification of the trees and their motion. In the well known example of Duffing's oscillator, such a classification does lead to the identification of hard and soft springs and also to interesting dynamics in different ranges of the parameters.²⁵

In this section, we analyze the potential energy of the system in detail by studying their fixed points and their stability. This will allow us to choose a range of parameters to work with in this study. For the two segment system, the potential energy, up to a constant, is

$$\begin{aligned}
 V(\theta_1, \theta_2) = & m_1g \left(\frac{\ell}{2} \cos \theta_1 \right) + m_2g \left(\ell \cos \theta_1 + \frac{\ell}{2} \cos \theta_2 \right) \\
 & + \frac{1}{2}k_1\theta_1^2 + \frac{1}{4}k_1\alpha_1\theta_1^4 + \frac{1}{2}k_2(\theta_2 - \theta_1)^2 \\
 & + \frac{1}{4}k_2\alpha_2(\theta_2 - \theta_1)^4. \tag{5}
 \end{aligned}$$

Here, we have considered the potential energy due to gravitation and the potential energy due to nonlinear restoring force. Note, as a matter of definition, that k_1 and k_2 are present in the anharmonic terms too.

Because of the gravitational term, there are infinite number of critical points, but we would restrict the values of θ_i to $-\pi < \theta_i < \pi$. Then, the maximum number of critical points we have is 9. A critical point (θ_1^*, θ_2^*) is obtained by solving

$$\frac{\partial V}{\partial \theta_1} = 0 \quad \text{and} \quad \frac{\partial V}{\partial \theta_2} = 0.$$

This leads to the equations

$$\begin{aligned}
 - \left(\frac{m_1}{2} + m_2 \right) g \ell \sin \theta_1 + k_1\theta_1 + k_1\alpha_1\theta_1^3 - k_2(\theta_2 - \theta_1) \\
 - k_2\alpha_2(\theta_2 - \theta_1)^3 = 0, \tag{6} \\
 - m_2g \frac{\ell}{2} \sin \theta_2 + k_2(\theta_2 - \theta_1) + k_2\alpha_2(\theta_2 - \theta_1)^3 = 0.
 \end{aligned}$$

We obtained the critical points numerically by finding the intersections of the zero level curves of the surfaces generated by these two equations. As expected geometrically, there are either 9, 5, 3, or 1 critical points for different range of parameter values. Then, the determinant of the Hessian matrix

$$D = \frac{\partial^2 V}{\partial \theta_1^2} \Big|_{(\theta_1^*, \theta_2^*)} \frac{\partial^2 V}{\partial \theta_2^2} \Big|_{(\theta_1^*, \theta_2^*)} - \left(\frac{\partial^2 V}{\partial \theta_2 \partial \theta_1} \Big|_{(\theta_1^*, \theta_2^*)} \right)^2 \tag{7}$$

was calculated at these critical points to determine their stability. It turns out that, as can be guessed from the geometrical reasoning, when there are 9 critical points four are stable and five are unstable and when there are 5 or 3 of them, two may be stable.

In order to understand the behavior away from the fixed points, we have plotted the function $V(\theta_1, \theta_2)$ for selected values of k_1 , k_2 , α_1 , and α_2 . Figure 1 depicts four representative shapes of the potential energy. The undamped motion is bounded in the case of types (a) and (c), whereas it is unbounded in the case of type (d). For the potential energy of the type (b), the motion is bounded only for a small range of initial conditions near the origin. As seen from the figure, the potential energy in (a) is bounded and also can have more than one attractor. We restrict ourselves to those parameter values which correspond to the potential energy as in (a). It is clear from the equation for the potential energy that whenever k_i 's and α_i 's have

the same sign, we are assured that the system is bounded. Thus, the possible combination of parameters for which bounded wells are present are as follows:

$$\begin{aligned}
 &k_1 > 0, k_2 > 0, \alpha_1 > 0, \alpha_2 > 0, \\
 &k_1 < 0, k_2 < 0, \alpha_1 < 0, \alpha_2 < 0, \\
 &k_1 > 0, k_2 < 0, \alpha_1 > 0, \alpha_2 < 0, \\
 &k_1 < 0, k_2 > 0, \alpha_1 < 0, \alpha_2 > 0.
 \end{aligned}
 \tag{8}$$

In the present work, we choose to work in the first combination where restoring coefficients are all positive.

It should be pointed out that it is not the case that only those potentials that guarantee the bounded motion as in (a) and (c) are of

interest for studying the swaying motion of trees. In fact, the potential of the type depicted in (b) can possibly naturally incorporate the breaking of trees. But such considerations are premature at this stage as the breaking of a tree does not seem to be clearly understood as yet.²⁶

IV. CHAOTIC PROPERTIES

This section focuses on exploring the chaotic properties of the two segment system. We study the system numerically for the values of k 's and α 's between 0 and 5. We confine ourselves to a realistic situation where the lower segment is more rigid so we always fix $k_1 = 5.0$ here. We have varied the values for other restoring coefficients α_1 , k_2 , and α_2 from 0.1 to 5.0. The damping coefficient b is kept constant at 0.5. The driving amplitude f takes the

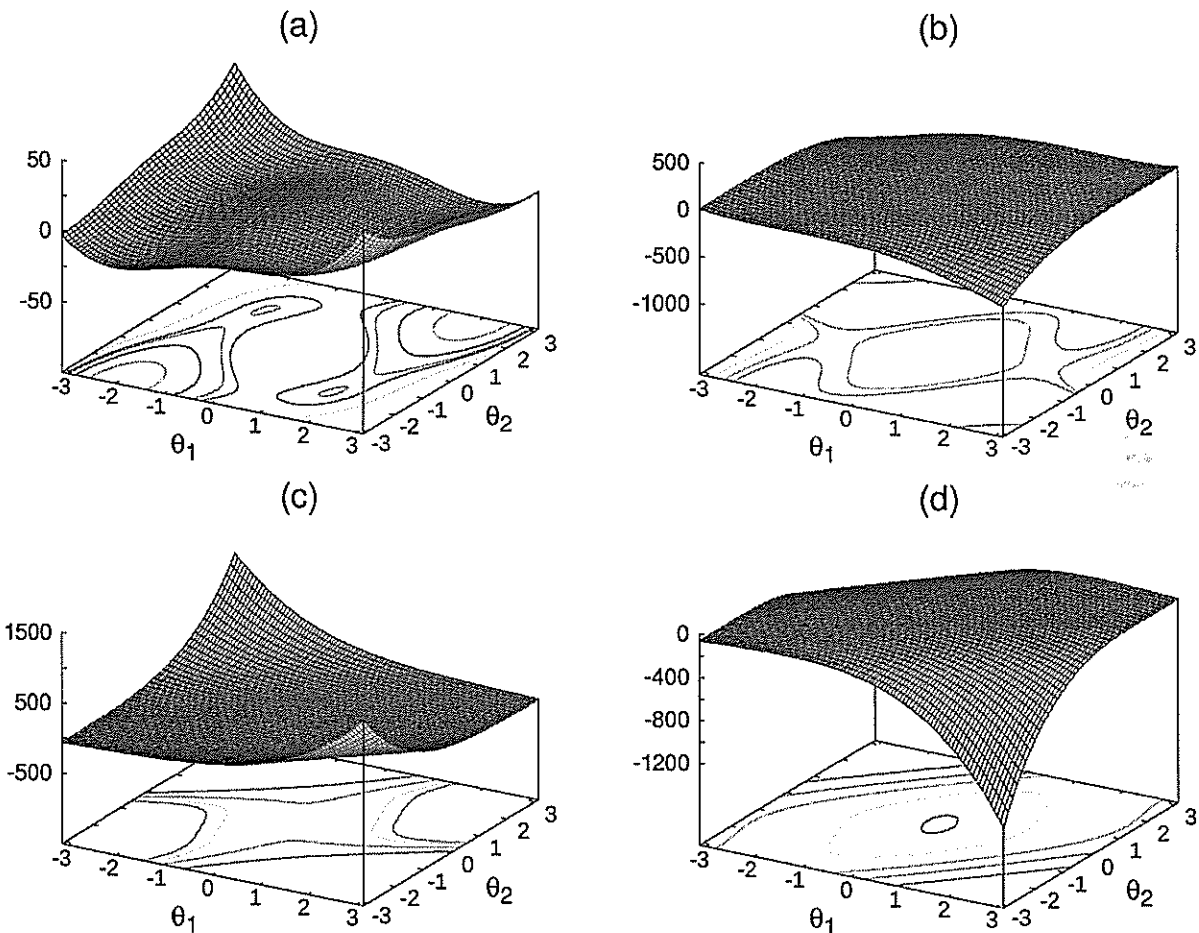


FIG. 1. The potential energy of the two segment chimney model. The motion of system is bounded in (a) ($k_1 = 5.0, \alpha_1 = 0.1, k_2 = 0.8, \alpha_2 = 0.1$) and (c) ($k_1 = 1.0, \alpha_1 = -1.0, k_2 = 1.0, \alpha_2 = 3.0$), unbounded in (d) ($k_1 = 1.0, \alpha_1 = -1.0, k_2 = 1.0, \alpha_2 = -3.0$) and may be either bounded or unbounded in (b) ($k_1 = 1.0, \alpha_1 = 2.0, k_2 = 1.0, \alpha_2 = -1.0$).

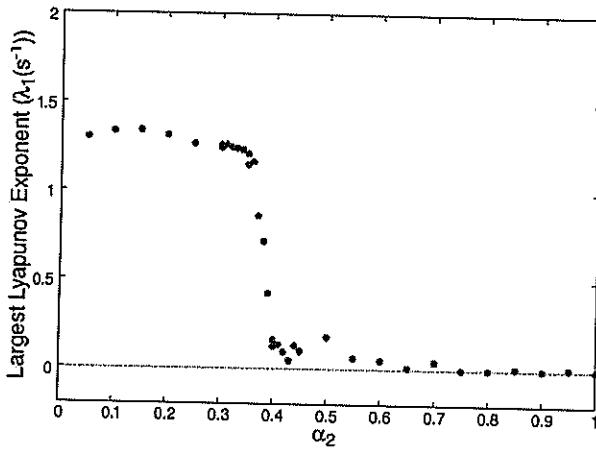


FIG. 2. Lyapunov exponent (λ_1) suddenly decreases with α_2 values for $\omega = 8$ and $k_1 = 5.0, \alpha_1 = 0.1, k_2 = 0.4, b = 0.5, f = 20$.

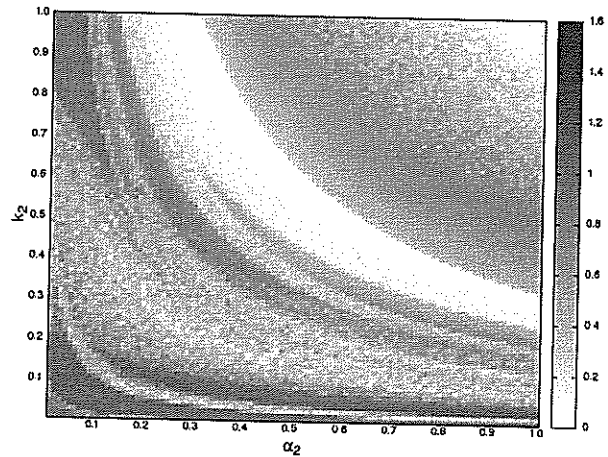


FIG. 3. Lyapunov exponent for $k_1 = 5.0, \alpha_1 = 0.1, b = 0.5, f = 10, \omega = 6$. The darker shade indicates the high value of the Lyapunov exponent, while the lighter shade indicates the low value.

values 8, 10, 15, and 20. The driving frequency ω is varied from 1 to 16. We found a chaotic solution for different parameter values. As discussed in Subsections IV A–IV C, the Lyapunov exponent is evaluated, and for a wide range of parameters, it is found to be positive. In some subregion of this parameter space, we also observed hyperchaos. Moreover, we observe that when the largest Lyapunov exponent reaches a certain threshold value there is also suppression of hyperchaos.

A. Lyapunov exponents

We calculated the Lyapunov spectrum using the algorithm proposed in Ref. 27. In Ref. 23, we had reported the Lyapunov exponent at few parameter values in order to show the difference between the approximate truncated gravitational potential¹⁷ vs the complete nonlinear term. We had observed a qualitatively different behavior. Here, the Lyapunov exponent is evaluated on a wide range of parameters and found to be positive, suggesting the existence of chaos for a large region of this parameter space. The largest Lyapunov exponent λ_1 is found to be maximum around $\omega = 3$. In general, the Lyapunov exponent increases with α_1, f and decreases with k_2, α_2 . That is, as the upper segment becomes stiffer, the system becomes less chaotic. In general, all these variations of the Lyapunov exponent we have discussed are more or less smooth. But, once in a while, we observed a sudden decline in the value of the Lyapunov exponent for high values of f and at driving frequency $\omega = 8$ as seen in Fig. 2. One implication of this result, for example, is that if the restoring coefficients of different branches have values spread around this particular value, then some branches will show more chaotic oscillations and some less for the same forcing. This is consistent with general observations. One does observe a variation in the movement of different branches. Earlier, this would have been naively attributed to the nonuniformity of the wind.

Generally, the variation of the Lyapunov exponent is monotonic with the parameters of the restoring forces, but there are

surprises too. Sometimes we observe some oscillatory behavior. For example, at $k_1 = 5.0, \alpha_1 = 0.1, b = 0.5, f = 10, \omega = 6$, as k_2 and α_2 are varied, we observed that there are some high–low–high–low bands of values of the Lyapunov exponent (λ_1) as shown in Fig. 3.

B. Hyperchaos

For small values of α_i 's, there exists a positive second largest Lyapunov exponent (λ_2), suggesting the existence of hyperchaos in the system. In general, when the largest Lyapunov exponent exceeds

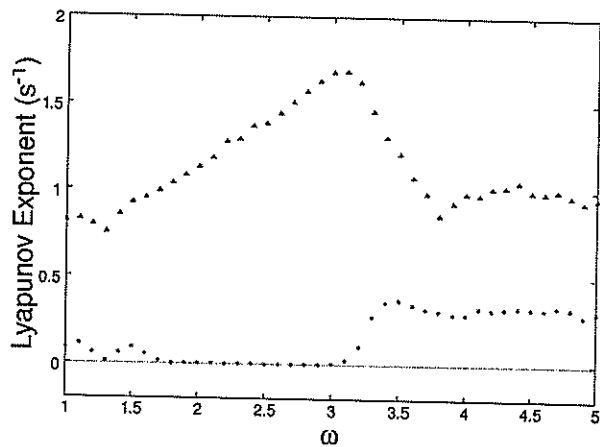


FIG. 4. Suppression of hyperchaos for $k_1 = 5.0, \alpha_1 = 0.1, k_2 = 0.8, \alpha_2 = 0.4, b = 0.5, f = 20$. The filled triangle denotes the largest Lyapunov exponent (λ_1), and filled circles are for the second largest Lyapunov exponent (λ_2).

0.5, the second largest Lyapunov exponent becomes positive. This second largest Lyapunov exponent usually follows the first one, *i.e.*, the hyperchaoticity of this two segment system increases with an increase in the values of parameters α_1 and f , while it decreases with the rise in the values of parameters k_2 and α_2 . Since chaoticity and hyperchaoticity both increase with α_1 , which means as the lower segment becomes more rigid, there is more chaos and hyperchaos in the system. The peak values of the second largest Lyapunov exponent (λ_2) are found to be around $\omega = 7$ or 8 . Just as there are high-low-high-low bands for λ_1 as shown in Fig. 3, we observed such bands for λ_2 also within the same parameter range.

C. Suppression of hyperchaos

As expected, when the largest Lyapunov exponent is greater than some threshold, we get hyperchaos. We also observed something interesting. When the largest Lyapunov exponent exceeds another higher threshold value, there is suppression of hyperchaos. That is, as λ_1 increases, λ_2 decreases and hits zero when λ_1 crosses this threshold value (see Fig. 4). Since the largest Lyapunov exponent is maximum at $\omega = 3$ or 4 , hyperchaos suppression is also observed within this frequency range. For outside this range of ω s, as stated earlier, for higher values of α_1 , the system is more chaotic and also hyperchaotic but not enough to cause the suppression of hyperchaos. With the increase in the values of α_1 and α_2 , the ω value where the suppression of hyperchaos is present shifts to higher values of ω .

V. SYNCHRONIZATION

In this section, we look at the synchronization^{26,27} between two segments. The existence of synchronization or the lack thereof will signify different types of swaying motion. It also might have implications to the internal stress generated within the branch and hence to breakage. Hence, we have studied synchronization between the lower and upper segments and found that phase synchronization exists for certain parameter values.

The synchronization between the segments is obtained by finding the linear correlation between θ_1 and θ_2 , which is measured in terms of Pearson's correlation coefficient ($\rho_{\theta_1\theta_2}$) as given below

$$\rho_{\theta_1\theta_2} = \frac{\text{cov}(\theta_1, \theta_2)}{\sigma_{\theta_1}\sigma_{\theta_2}}, \tag{9}$$

where $\text{cov}(\theta_1, \theta_2)$ is the covariance and σ_{θ_1} and σ_{θ_2} are standard deviations of θ_1 and θ_2 , respectively. $\rho_{\theta_1\theta_2}$ has values between $+1$ and -1 , where 1 implies absolute synchronization, 0 implies no synchronization, and -1 implies antisynchronization. We would like to report that we observe both the phase synchronization for some range of parameters, which changes over to antisynchronization at certain values of the parameters. We should emphasize that the synchronization occurs irrespective of whether the system is periodic or chaotic. In fact, we observe synchronization even when the system is hyperchaotic.

There are two different mechanisms of synchronization possible here. First of all, there is a common forcing. Both segments are driven by the same periodic force. Second, there is a bidirectional coupling between the two segments. We observe that when the synchronized motion is periodic, its frequency is the same as that of the drive, indicating the crucial role played by the drive. However, when the synchronized motion is chaotic (or hyperchaotic), then clearly mutual coupling dominates the motion.

It is observed that at low ω values, the system is in the synchronous state and as the ω increases, the synchronizing state of the system may change. We found three different types of transitions between synchronous state ($\rho_{\theta_1\theta_2} > 0.5$) and antisynchronous state ($\rho_{\theta_1\theta_2} < -0.5$) as shown in Fig. 5. The system either remains in the synchronous state for all ω values studied (type-1) as in Fig. 5(a), or it is in the synchronous state for small ω values. As ω increases, there is a sharp transition to the antisynchronous state and then remains in that state (type-2) as in Fig. 5(b), or the system keeps toggling between the synchronous state and the antisynchronous state (type-3) as in Fig. 5(c).

For the second case, the ω values at which the transition occurs shifts little toward higher ω values as we increase any parameter among α_1 , k_2 , and α_2 .

Different types are seen for different ranges of the parameters. In Fig. 6, we depict which type of transition occurs for different ranges of parameters. Here, the light gray region shows type-1, the medium gray region indicates type-2, and the dark gray represents type-3 of transition. It is found that with an increase in k_2 and α_2 , type-1 transition changes to type-3 transition, which then further changes to type-2 transition. Whereas with the increase in α_1 , type-2 transition changes to type-3 transition that further goes into type-1 transition.

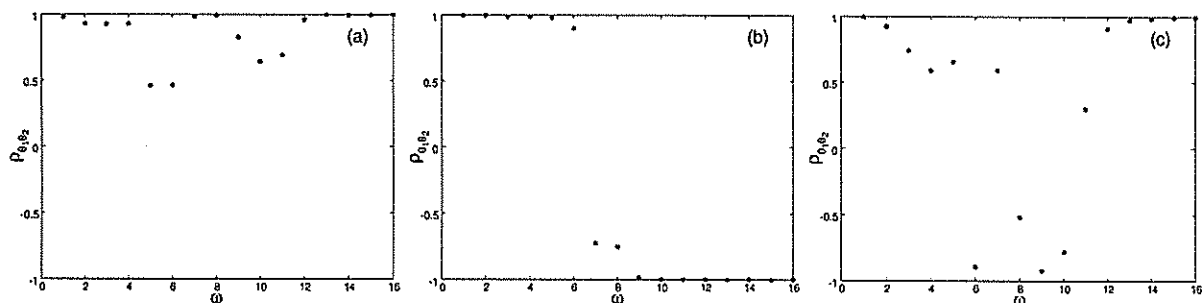


FIG. 5. The types of transitions between the synchronous state and the antisynchronous state. In (a), the system is always in a synchronous state (type-1), in (b) the system sharply changes its state from synchronous to antisynchronous (type-2), and in (c), the system toggles between the synchronous state and the antisynchronous state (type-3).

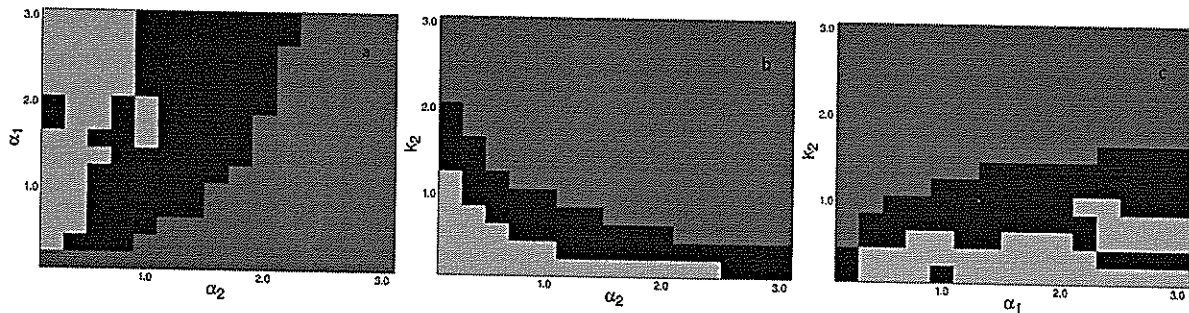


FIG. 6. Variation of different types of transitions with parameters α_1 , k_2 , and α_2 . Here, the light gray area shows the type-1, the medium gray region indicates the type-2, and the dark gray represents type-3 of transition. (a) at parameters $k_1 = 5.0$, $k_2 = 0.8$, $b = 0.5$, $f = 8$, (b) at parameter $k_1 = 5.0$, $\alpha_1 = 0.8$, $b = 0.5$, $f = 8$ and (c) at parameters $k_1 = 5.0$, $\alpha_2 = 0.8$, $b = 0.5$, $f = 8$.

These observations can be understood as follows. When the values of k_2 and/ or α_2 become large, that is, when the restoring force of the second segment increases it can possibly have its motion different from the first segment (antiphase motion for large ω). This might mean that, since we have fixed $k_1 = 5$, the lower segment could be playing a dominating role when the motion is synchronized, and the values of k_2 and α_2 are small.

VI. CONCLUSION

This work takes the next step in our systematic development of the nonlinear chimney model in order to understand the swaying motion of trees. We studied a special case of the model where two segments are connected end to end and of which one is pivoted at the end to a rigid support. There is a nonlinear restoring force at both joints and a gravitational force in the opposite direction.

We have explored this model in some detail with focus on the nonlinear dynamical properties that might have relevance in understanding the swaying motions of trees. First, we studied the chaotic properties and found that chaos does exist for a wide range of parameters. Moreover, over a substantial range of parameters, we observed hyperchaos too. Then, we noticed a curious phenomenon, which we call suppression of hyperchaos, where at some parameter values one positive Lyapunov exponent increases beyond a threshold and the other decreases and goes to zero. Then, we also studied synchronization between the two segments and found that the system does show phase synchronization, as characterized by the Pearson coefficient, for some parameter values and antisynchronization for others even when the solution is chaotic.

The chaotic nature of the motion, possibly along with the lack of synchronization, might have implications for the breaking off a branch or a tree. The phenomenon of breaking is not yet well understood.¹⁴ Resonance is thought of as a possible reason, but it is not adequate. Surprisingly, the nonlinear phenomena have not yet been incorporated in attempts to understand the swaying motion of trees in general and breaking in particular. Hopefully, this work will add a new dimension to the discussion.

The future generalizations will either proceed in the direction of a longer linear chain to resemble grasses or toward a branched structure to model plants. Also, incorporating the biological inputs

in the form of the values of the parameters and comparison with actual experiments will have to be carried out.

ACKNOWLEDGMENTS

K.M.K. and A.R.V.K. would like to acknowledge the Science and Engineering Research Board (No. EMR/2014/000255), India, for financial assistance during this work. A.R.V.K. would also like to acknowledge University Grants Commission (JRF) fellowship during a part of this work.

DATA AVAILABILITY

The data that support the findings of this study are available from the corresponding author upon reasonable request.

REFERENCES

- Gardiner, P. Berry, and B. Moulia, "Review: Wind impacts on plant growth, mechanics and damage," *Plant. Sci.* **245**, 94–118 (2016).
- M. S. Watt, J. R. Moore, and B. McKinlay, "The influence of wind on branch characteristics of *Pinus radiata*," *Trees* **19**, 58–65 (2005).
- S. Fathi, L. Bejo, and F. Divos, "Investigating the effect of weather and seasonal factors on root stability using dynamic measurements," *Open J. For.* **10**, 124–134 (2020).
- J. Diener, M. Rodriguez, L. Baboud, and L. Reveret, "Wind projection basis for real-time animation of trees," *Comput. Graph. Forum* **28**, 533–540 (2009).
- Y. Akagi and K. Kitajima, "Computer animation of swaying trees based on physical simulation," *Comput. Graph.* **30**, 529–539 (2006).
- N. J. Oliapuram and S. Kumar, "Realtime forest animation in wind," in *ICVGIP '10: Proceedings of the Seventh Indian Conference on Computer Vision, Graphics and Image Processing* (2010), Vol. 10, pp. 197–204.
- R. Habel, A. Kusternig, and M. Wimmer, "Physically guided animation of trees," *Comput. Graph. Forum* **28**, 523–533 (2009).
- E. De Langre, "Effects of wind on plants," *Annu. Rev. Fluid Mech.* **40**, 141–168 (2008).
- A. Hassinen, M. Lemettinen, H. Peltola, S. Kellomaki, and B. Gardiner, "A prism-based system for monitoring the swaying of trees under wind loading," *Agric. For. Meteorol.* **90**, 187–194 (1998).
- D. Sellier, T. Fourcaud, and P. Lac, "A finite element model for investigating effects of aerial architecture on tree oscillations," *Tree Phys.* **26**, 799–806 (2006).
- A. Barbacci, J. Diener, P. Hemon, B. Adam, N. Dones, L. Reveret, and B. Moulia, "A robust videogrametric method for the velocimetry of wind induced motion in trees," *Agric. For. Meteorol.* **184**, 220–229 (2013).

- ¹²J. R. Moore and D. A. Maguire, "Natural sway frequencies and damping ratios of trees: Influence of crown structure," *Trees* **19**, 363–373 (2005).
- ¹³E. De Langre *et al.*, "Nondestructive and fast vibration phenotyping of plants," *Plant Phenom.* **2019**, 1–10 (2019).
- ¹⁴T. Jackson *et al.*, "An architectural understanding of natural sway frequencies in trees," *J. R. Soc. Interface* **16**, 20190116 (2019).
- ¹⁵T. Kerzenmacher and B. Gardiner, "A mathematical model to describe the dynamic response of a spruce tree to the wind," *Trees* **12**, 385–394 (1998).
- ¹⁶J. Vincent, *Structural Biomaterials* (Princeton University Press, Princeton, 1990).
- ¹⁷L. Miller, "Structural dynamics and resonance in plants with nonlinear stiffness," *J. Theor. Biol.* **234**, 512–524 (2005).
- ¹⁸K. D. Murphy and M. Rudnicki, "A physics-based link model for tree vibrations," *Am. J. Bot.* **99**, 1918–1929 (2012).
- ¹⁹B. Theckes, E. de Langre, and X. Boutillon, "Damping by branching: A bioinspiration from trees," *Bioinspir. Biomim.* **6**, 1–11 (2011).
- ²⁰E. R. Fankem, B. R. N. Nbenjo, P. Wofo, and U. Dorka, "An inverted pendulum with multibranching view as self-controlled system: Modelling and vibration absorber capacity," *J. Vib. Control* **26**, 1–11 (2020).
- ²¹I. Kovacic, M. Zukovic, and D. Radomirovic, "On a localization phenomenon in two types of bio-inspired hierarchically organized oscillatory systems," *Nonlinear Dyn.* **99**, 679–706 (2020).
- ²²S. Ota, M. Tamura, K. Fujita, T. Fujimoto, K. Muraoka, and N. Chiba, "1/f^β noise-based real-time animation of trees swaying in wind fields," in *Proceedings of Computer Graphics International Conference, CGI (2003)*, pp. 52–59.
- ²³A. R. V. Kashyap and K. M. Kolwankar, "Chaotic properties of single element nonlinear chimney model: Effect of directionality," *Int. J. Bifurc. Chaos* **29**, 1950048 (2019).
- ²⁴S. J. Patil, A. R. V. Kashyap, and K. M. Kolwankar, "Homotopy analysis method for oscillatory systems with cubic and trigonometric non-linearity," in *Proceedings of CMNA 2018* (Springer, 2020).
- ²⁵M. Lakshmanan and K. Murali, "Duffing oscillator: bifurcation and chaos," in *Chaos in Nonlinear Oscillators: Controlling and Synchronization*, World Scientific Series on Nonlinear Science Vol. 13, edited by L. O. Chua (World Scientific, 1996), pp. 35–66.
- ²⁶J. Moore, B. Gardiner, and D. Sellier, "Tree mechanics and wind loading," in *Plant Biomechanics*, edited by A. Geitmann and J. Gril (Springer, Cham, 2018), pp. 79–106.
- ²⁷A. Wolf, J. B. Swift, H. L. Swinney, and J. A. Vastano, "Determining Lyapunov exponents from a time series," *Physica D* **16**, 285–317 (1985).
- ²⁸A. Pikovsky, M. Rosenblum, and J. Kurth, *Synchronization: A Universal Concept in Nonlinear Dynamics* (Cambridge University Press, 2001).
- ²⁹S. Boccaletti, J. Kurths, G. Osipov, D. L. Valladares, and C. S. Zhou, "The synchronization of chaotic systems," *Phys. Rep.* **366**, 1–101 (2002).

Certified as
TRUE COPY


Principal
Ramniranjan Jhunjhunwala College,
Ghatkopar (W), Mumbai-400086.